Glueball production in high-energy collisions

L. Houra-Yaou, P. Kessler, and J. Parisi

Laboratoire de Physique Corpusculaire, Collège de France, Paris, France

(Received 11 June 1991)

Using a nonrelativistic gluon bound-state model, we compute the subprocesses $qg \rightarrow qG$, $q\bar{q} \rightarrow gG$, $gg \rightarrow gG$, and their contribution to the overall reaction $p\bar{p} \rightarrow \text{jet} + \text{glueball} + X$, assuming that the glueball G and the quark (gluon) jet are emitted with their transverse momenta large (> 10 GeV), opposite, and approximately equal. We show that, for present glueball candidates and for their possible quantum states, fairly large predictions are obtained, thus justifying future experiments of this type that might be performed at high-energy $p\bar{p}$ or pp colliders, such as the CERN S$p\bar{p}$S or the Fermilab Tevatron.

I. INTRODUCTION

While the existence of glueballs is considered a crucial test of quantum chromodynamics [1] and after a few candidates for such particles have emerged from various experiments over the last years [2], further experimental evidence is still needed in order firmly to establish their nature and properties.

It is generally agreed that glueballs should be looked for in reactions involving a gluon-rich environment, such as radiative J/ψ decay and diffractive hadron-hadron scattering corresponding to double Pomeron exchange (the Pomeron being assumed to have a multigluon structure). The basic idea of this paper is that hard collisions occurring in high-energy reactions may provide another means of creating that kind of environment and, consequently, of making glueballs.

We here consider the reaction

$$p\bar{p} \rightarrow \text{jet} + \text{glueball} + X \ ,$$

involving the hard-collision subprocesses (i) $qg \rightarrow qG$, (ii) $q\bar{q} \rightarrow gG$, and (iii) $gg \rightarrow gG$, where G is the glueball considered. We assume the quark (gluon) jet and glueball to be emitted at large, opposite, and approximately equal transverse momenta. Such a reaction may be studied, in particular, at high-energy $p\bar{p}$ colliders: the CERN S$p\bar{p}$S or the Fermilab Tevatron.

Actually, that kind of investigation was already suggested a few years ago by other authors [3], and some numerical predictions were provided by them. However, in their computations they used a model involving two collinear gluons, which means that implicitly they restricted their study to the production of glueballs (digluons) with $L = 0$, L being the quantum number of the orbital angular momentum.

In order to be able to treat the case of digluons with any value of L (in particular $L = 0$, 1, or 2), we here use an extension of the nonrelativistic gluon bound-state model, previously applied to the computation of 2γ decay widths of glueballs [4]. That extended model is exhibited in Sec. II. We then apply it in Sec. III in order to predict the transverse-momentum spectra that should be pro-

duced in the above-mentioned reaction, considering various glueball candidates and their possible quantum states. Section IV contains a discussion of our results and a brief conclusion. Details of our calculation are given in two Appendixes.

II. EXTENSION OF THE NONRELATIVISITC BOUND-STATE MODEL

As in Ref. [4], we limit ourselves to glueballs made up of two gluons. While in that paper only reactions of the type $ab \leftrightarrow G$ were considered, the processes we are going to study are of the type $ab \rightarrow cG$ [Fig. 1(a)]. In analogy with the procedure outlined in Ref. [4] (which was inspired by a similar model used by other authors for ordinary mesons, i.e., quarkonia; see, e.g., Refs. [5,6]), the
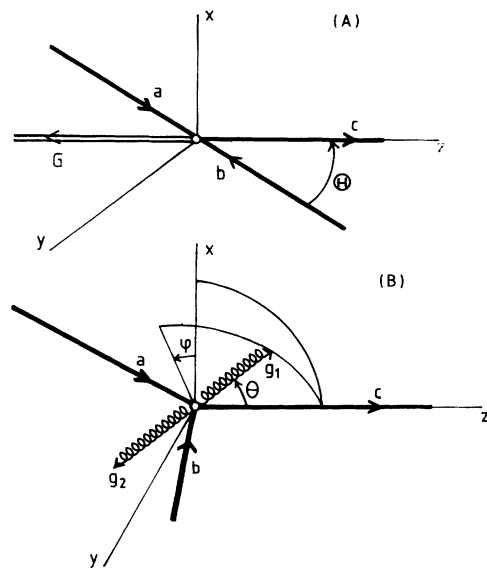
FIG. 1. Kinematic schemes (a) for the process $ab \rightarrow cG$ in the center-of-mass frame of a and b (frame A) and (b) for the process $ab \rightarrow cg_1 g_2$ in the center-of-mass frame of g_1 and g_2 (frame B).

helicity amplitudes of that process are derived from the corresponding amplitudes of the elementary process $ab \rightarrow cgg$. In order to achieve that derivation, we perform a Lorentz transformation along the z axis of Fig. 1(a), moving from the center-of-mass frame of the ab collision (hereafter called frame A) to the glueball rest frame, i.e., the c.m. frame of the gluons g_1, g_2 [henceforth called frame B; see Fig. 1(b)]. As in Ref. [4], we assume that either gluon tends to take half of the glueball mass.

We are now going to derive the basic formula we shall apply in this study. We start from the prescription (similar to formula (2.1) of Ref.[6])

$$\mathcal{M}_{ab \rightarrow cG} = \left[\frac{2}{M} \right]^{1/2} \int \frac{d^3p}{(2\pi)^{3/2}} \Psi^*(\mathbf{p}) \mathcal{M}_{ab \rightarrow cg_1g_2} , \tag{1}$$

where M is the glueball mass; $\Psi(p)$ is the glueball wave function, defined in frame B; $\mathbf{p}$ ($-\mathbf{p}$) is, in that frame, the three-momentum of either gluon. In accordance with the nonrelativistic assumption, $\Psi(p)$ is nonzero only near the value $p = 0$ (defining $p = |\mathbf{p}|$).

Note that the glueball is characterized by the following quantum numbers: total spin J, orbital angular momentum L, intrinsic spin $S (\leq 2)$, and in addition by Λ, the component of J on the z axis.

The wave function factorizes into a radial function times a spherical harmonic:

$$\Psi^*(\mathbf{p}) = R_L(p) Y^*_{L\Lambda_L}(\theta, \varphi) , \tag{2}$$

where Λ_L is the component of L on the z axis, while θ and φ are the orbital and azimuthal angles defined in Fig. 1(b). One thus gets

$$\mathcal{M}_{ab \rightarrow cG} = \left[\frac{2}{M} \right]^{1/2} \int \frac{p^2 dp}{(2\pi)^{3/2}} R_L(p) \int d(\cos\theta) d\varphi \, Y^*_{L\Lambda_L}(\theta, \varphi) \mathcal{M}_{ab \rightarrow cg_1g_2} . \tag{3}$$

What remains unwritten in formula (3) is the dependence of both amplitudes $\mathcal{M}_{ab \rightarrow cG}$ and $\mathcal{M}_{ab \rightarrow cg_1g_2}$ on the total energy E and the scattering angle Θ, both defined in frame A, and in addition on the glueball quantum numbers J, L, S, Λ as well as on the helicities $\lambda_a, \lambda_b, \lambda_c$ (conveniently defined in frame B) of particles a, b, c, respectively. Finally, $\mathcal{M}_{ab \rightarrow cg_1g_2}$ yet depends on Λ_L, and a summation over Λ_L is implicit on the right-hand side of Eq. (3).

Introducing in addition the helicities λ_1, λ_2 (defined in frame B) of the gluons g_1, g_2, the following relation connects the above-defined amplitude $\mathcal{M}_{ab \rightarrow cg_1g_2}$ with the corresponding helicity amplitude characterized by λ_1, λ_2:

$$\mathcal{M}_{ab \rightarrow cg_1g_2} = \langle LS\Lambda_L\Lambda_S | LSJ\Lambda \rangle d^S_{\Lambda_S\overline{\Lambda}}(\theta) e^{-i\Lambda_S\varphi} \sum_{\lambda_1\lambda_2} \langle 11\lambda_1 - \lambda_2 | 11S\overline{\Lambda} \rangle \mathcal{M}^{\lambda_1\lambda_2}_{ab \rightarrow cg_1g_2}(\theta, \varphi) , \tag{4}$$

where we have applied the usual notations of angular momentum theory [7], i.e., $\langle j_1j_2m_1m_2 | j_1j_2JM \rangle$ for Clebsch-Gordan coefficients, while $d^S_{\Lambda_S\overline{\Lambda}}$ is a Wigner rotation matrix element. We have called Λ_S the component of S on the z axis and $\overline{\Lambda}$ its component on the gluon emission axis in frame B; note $\Lambda_S = \Lambda - \Lambda_L$, $\overline{\Lambda} = \lambda_1 - \lambda_2$. Using the relations [8]

$$Y^*_{L\Lambda_L}(\theta, \varphi) = \left[\frac{2L+1}{4\pi} \right]^{1/2} d^L_{\Lambda_L 0}(\theta) e^{-i\Lambda_L\varphi} , \tag{5}$$

$$\sum_{\Lambda_L} d^L_{\Lambda_L 0}(\theta) d^S_{\Lambda_S\overline{\Lambda}}(\theta) \langle LS\Lambda_L\Lambda_S | LSJ\Lambda \rangle = d^J_{\Lambda\overline{\Lambda}}(\theta) \langle LS0\overline{\Lambda} | LSJ\overline{\Lambda} \rangle , \tag{6}$$

and combining them with (3) and (4), one gets

$$\mathcal{M}_{ab \rightarrow cG} = \left[\frac{2}{M} \right]^{1/2} \int \frac{p^2 dp}{(2\pi)^{3/2}} R_L(p) \int d(\cos\theta) d\varphi \sum_{\lambda_1\lambda_2} \chi^{LSJ\Lambda}_{\lambda_1\lambda_2}(\theta, \varphi) \mathcal{M}^{\lambda_1\lambda_2}_{ab \rightarrow cg_1g_2} , \tag{7}$$

where the angular projection function $\chi^{LSJ\Lambda}_{\lambda_1\lambda_2}(\theta, \varphi)$ is given by

$$\chi^{LSJ\Lambda}_{\lambda_1\lambda_2}(\theta, \varphi) = \left[\frac{2L+1}{4\pi} \right]^{1/2} d^J_{\Lambda\overline{\Lambda}}(\theta) e^{-i\Lambda\varphi} \langle LS0\overline{\Lambda} | LSJ\overline{\Lambda} \rangle \langle 11\lambda_1 - \lambda_2 | 11S\overline{\Lambda} \rangle . \tag{8}$$

On the other hand, a number of algebraic manipulations proceeding from a Fourier transformation [see formulas (2.2)–(2.5), and (2.11) in Ref. [6]] lead to the relation

$$\int \frac{p^2 dp}{(2\pi)^{3/2}} p^L R_L(p) = \frac{(-i)^L(2L+1)}{4\pi L!} \left[\frac{d^L}{dr^L} R_L(r) \right]_{r=0} , \tag{9}$$

where $R_L(r)$ is the radial wave function in configuration space. Therefrom, one is led to

$$\mathcal{M}_{ab \rightarrow cG} = \left[\frac{2}{M} \right]^{1/2} (-i)^L \frac{(2L+1)!!}{L!} \left[\frac{d^L}{dr^L} R_L(r) \right]_{r=0} \frac{1}{p^L} \int \frac{d(\cos\theta) d\varphi}{4\pi} \sum_{\lambda_1\lambda_2} \chi^{LSJ\Lambda}_{\lambda_1\lambda_2}(\theta, \varphi) \mathcal{M}^{\lambda_1\lambda_2}_{ab \rightarrow cg_1g_2}(\theta, \varphi) . \tag{10}$$

Here the dependence on p that appears on the right-hand side is fictitious since, because of the presence of the angular projection function that fixes L, the integral on the right-hand side is proportional to p^L (neglecting higher-order powers of p, since p is bound to remain close to zero). Setting $p \simeq M\beta/2$, where β is the velocity of either gluon in frame B, we finally get the formula

$$\mathcal{M}_{ab \to cG}^{\lambda_a \lambda_b, \lambda_c \Lambda} = (-i)^L \left[\frac{2}{M} \right]^{L+1/2} \frac{(2L+1)!!}{L!} \left[\frac{d^L}{dr^L} R_L(r) \right]_{r=0} \lim_{\beta \to 0} \frac{1}{\beta^L} \int \frac{d(\cos\theta)\, d\varphi}{4\pi} \sum_{\lambda_1 \lambda_2} \chi_{\lambda_1 \lambda_2}^{LSJ\Lambda}(\theta, \varphi) \mathcal{M}_{ab \to cg_1 g_2}^{\lambda_a \lambda_b, \lambda_c \lambda_1 \lambda_2}(\theta, \varphi) \; ,$$

(11)

where we have explicitly introduced the helicities of all particles involved as superscripts of the corresponding amplitudes.

That relation is the generalization of formula (1) of Ref. [4], which is the analogue of formula (2.12) of Ref. [6]. Before we apply it in the next section, let us remark that our model may be considerably simplified when $L = 0$. In that case one may simply set $\beta = 0$ in the computation of the process $ab \to cg_1 g_2$, which means that both gluons are set at rest in frame B. Then, calling λ, λ' their spin components on the z axis, formula (4) may be replaced by

$$\mathcal{M}_{ab \to cg_1 g_2} = \sum_{\lambda \lambda'} \langle 11\lambda\lambda' | 11J\Lambda \rangle \mathcal{M}_{ab \to cg_1 g_2}^{\lambda \lambda'} \; ,$$

(12)

and consequently formula (11) may be replaced by

$$\mathcal{M}_{ab \to cG}^{\lambda_a \lambda_b, \lambda_c \Lambda} = \frac{1}{\sqrt{2\pi M}} R_0^*(r=0)$$

$$\times \sum_{\lambda \lambda'} \langle 11\lambda\lambda' | 11J\Lambda \rangle \mathcal{M}_{ab \to cg_1 g_2}^{\lambda_a \lambda_b, \lambda_c \lambda \lambda'} \; .$$

(13)

Since there is no dependence any more, on the right-hand side, on θ and φ, the whole computation may be performed in frame A (and all helicities defined in that frame). The formalism thus applied then becomes very similar to the one introduced by Brodsky and Lepage [9] for the computation of exclusive processes involving ordinary $(q\bar{q})$ mesons with $L = 0$.

Before closing this section, let us add a remark: A general formalism for prompt production of mesons with any value of angular momentum has been developed by Benayoun and Froissart [10]. With respect to that general treatment, the specificity of the model here used is that (i) we treat the constituent partons (in our case gluons) as nonrelativistic $(\beta \to 0)$ in the meson rest frame, and (ii) we assume their masses to be equal. This allows us to minimize the number of free parameters in our calculation; eventually, we will reduce it to zero by using radiative J/ψ decay for normalization.

III. APPLICATION
TO THE REACTION $p\bar{p} \to \mathrm{JET} + \mathrm{GLUEBALL} + X$

We shall now apply our model, i.e., basically formula (11), to the computation of the three subprocesses contributing to the reaction considered.

A. Contribution of the subprocess $qg \to q'G$

We here compute the Feynman graphs (1)–(7) of Fig. 2, describing the process $qg \to q'g_1 g_2$. The contribution of each graph, except (7), will be doubled by exchanging g_1 and g_2.

Denoting all momentum four-vectors like the corresponding particles, defining $\varepsilon^{\lambda_g}, \varepsilon_1^{\lambda_1}, \varepsilon_2^{\lambda_2}$ as the polarization four-vectors of g, g_1, g_2, respectively, and $u^{\lambda_q}, u'^{\lambda_{q'}}$ as the spinors for q, q', using the notation $\tilde{a} = a_\mu \gamma^\mu$, we write the corresponding helicity amplitudes as
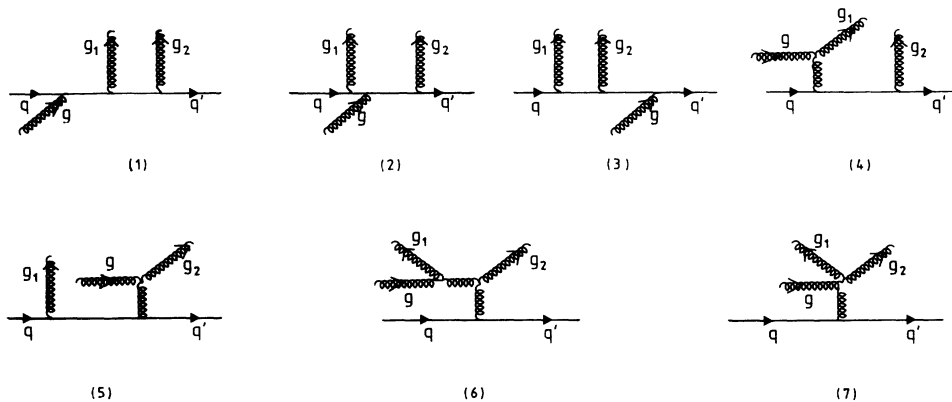
FIG. 2. Feynman graphs for the subprocess $qg \to q'g_1 g_2$. Other graphs, providing the same contribution to the helicity amplitudes of the subprocess $qg \to q'G$, are derived from those here represented (except for graph 7) by exchanging g_1 and g_2.

$$\mathcal{M}_{(1)}^{\lambda_q\lambda_g,\lambda_{q'}\lambda_1\lambda_2} = -\tfrac{4}{3}\mathrm{Tr}[u^{\lambda_q}\bar{u}'^{\lambda_{q'}}\varepsilon_2^{*\lambda_2}(\bar{q}'+\tilde{g}_2)^{-1}\varepsilon_1^{*\lambda_1}(\bar{q}+\tilde{g})^{-1}\varepsilon^{\lambda_g}] , \tag{14}$$

$$\mathcal{M}_{(2)}^{\lambda_q\lambda_g,\lambda_{q'}\lambda_1\lambda_2} = \tfrac{1}{6}\mathrm{Tr}[u^{\lambda_q}\bar{u}'^{\lambda_{q'}}\varepsilon_2^{*\lambda_2}(\bar{q}'+\tilde{g}_2)^{-1}\varepsilon^{\lambda_g}(\bar{q}-\tilde{g}_1)^{-1}\varepsilon_1^{*\lambda_1}] , \tag{15}$$

$$\mathcal{M}_{(3)}^{\lambda_q\lambda_g,\lambda_{q'}\lambda_1\lambda_2} = -\tfrac{4}{3}\mathrm{Tr}[u^{\lambda_q}\bar{u}'^{\lambda_{q'}}\varepsilon^{\lambda_g}(\bar{q}'-\tilde{g})^{-1}\varepsilon_2^{*\lambda_2}(\bar{q}-\tilde{g}_1)^{-1}\varepsilon_1^{*\lambda_1}] , \tag{16}$$

$$\mathcal{M}_{(4)}^{\lambda_q\lambda_g,\lambda_{q'}\lambda_1\lambda_2} = \tfrac{3}{2}\mathrm{Tr}[u^{\lambda_q}\bar{u}'^{\lambda_{q'}}\varepsilon_2^{*\lambda_2}(\bar{q}'+\tilde{g}_2)^{-1}\gamma^\mu][2(g\cdot\varepsilon_1^*)\varepsilon_\mu^{\lambda_g}-(\varepsilon^{\lambda_g}\cdot\varepsilon_1^{*\lambda_1})(g+g_1)_\mu+2(g_1\cdot\varepsilon^{\lambda_g})\varepsilon_{1\mu}^{*\lambda_1}](g-g_1)^{-2} , \tag{17}$$

$$\mathcal{M}_{(5)}^{\lambda_q\lambda_g,\lambda_{q'}\lambda_1\lambda_2} = \tfrac{3}{2}\mathrm{Tr}[u^{\lambda_q}\bar{u}'^{\lambda_{q'}}\gamma^\mu(\bar{q}-\tilde{g}_1)^{-1}\varepsilon_1^{*\lambda_1}][-2(g_2\cdot\varepsilon^{\lambda_g})\varepsilon_{2\mu}^{*\lambda_2}+(\varepsilon^{\lambda_g}\cdot\varepsilon_2^{*\lambda_2})(g+g_2)_\mu-2(g\cdot\varepsilon_2^*)\varepsilon_\mu^{\lambda_g}](g-g_2)^{-2} , \tag{18}$$

$$\mathcal{M}_{(6)}^{\lambda_q\lambda_g,\lambda_{q'}\lambda_1\lambda_2} = -3\,\mathrm{Tr}(u^{\lambda_q}\bar{u}'^{\lambda_{q'}}\gamma^\mu)[(g_2-g_1+g)_\mu\varepsilon_2^{*\lambda_2}+2(g_1-g)\cdot\varepsilon_2^{*\lambda_2}g_{\mu\nu}+\varepsilon_{2\mu}^{*\lambda_2}(g-g_1-2g_2)_\nu]$$

$$\times[(\varepsilon_1^{*\lambda_1}\cdot\varepsilon^{\lambda_g})(g_1+g)^\nu-2(g\cdot\varepsilon_1^{*\lambda_1})\varepsilon^{\lambda_g\nu}-2(g_1\cdot\varepsilon^{\lambda_g})\varepsilon_1^{*\lambda_1\nu}](g-g_1)^{-2}(q-q')^{-2} , \tag{19}$$

$$\mathcal{M}_{(7)}^{\lambda_q\lambda_g,\lambda_{q'}\lambda_1\lambda_2} = 3\,\mathrm{Tr}(u^{\lambda_q}\bar{u}'^{\lambda_{q'}}\gamma^\mu)[2(\varepsilon_1^{*\lambda_1}\cdot\varepsilon_2^{*\lambda_2})\varepsilon_\mu^{\lambda_g}-(\varepsilon^{\lambda_g}\cdot\varepsilon_1^{*\lambda_1})\varepsilon_{2\mu}^{*\lambda_2}-(\varepsilon^{\lambda_g}\cdot\varepsilon_2^{*\lambda_2})\varepsilon_{1\mu}^{*\lambda_1}](q-q')^{-2} . \tag{20}$$

Here we have left aside coupling constants, as well as a color factor $1/(4\sqrt{2})\lambda_{jl}^a$, where λ_{jl}^a are elements of the Gell-Mann matrices [11], a being the color index of the incident gluon and j,l those of the quarks q,q'. Let us note that, taking massless quarks, "helicity conservation" as defined by Brodsky and Lepage [9] entails $\lambda_q=\lambda_{q'}$. In addition, we may restrict ourselves to the case $\lambda_q=\lambda_{q'}=+\tfrac{1}{2}$ since we know that, because of angular momentum and parity conservation, once we have derived the helicity amplitudes of the two-body process $qg\rightarrow q'G$, reversing all helicities always leads to the same expression of the amplitude (apart from the sign). The spinor product that appears in formulas (14)–(20) is then expressed (in frame B) by

$$u^{1/2}\bar{u}'^{1/2} = \frac{(E^2-M^2)^{1/2}}{4M}(I+\gamma_5)$$

$$\times[(\gamma_0-\gamma_3)E\bar{c}+(\gamma_1-i\gamma_2)M\bar{s}] , \tag{21}$$

where we define $\bar{c}=\cos\Theta/2$, $\bar{s}=\sin\Theta/2$.

Our calculation is considerably simplified by introducing the parameter $\eta=M/E$ and noting that, under realistic conditions of a high-energy experiment (i.e., assuming a transverse momentum of at least 10 GeV for the glueball and the quark jet), η remains small (≤ 0.1), so that we may make a series expansion in powers of η and keep only the lowest-order term.

Computing the amplitudes (14)–(20) while using that simplification, summing up those amplitudes, and then applying formula (11), we are led to the expressions of the helicity amplitudes $\mathcal{M}_{qg\rightarrow q'G}^{\lambda_q\lambda_g,\lambda_{q'}\Lambda}$ that are given in Appendix A for the glueball quantum states we are considering (the same states as in Ref. [4]). We may remark that, at lowest order in η (i.e., at order η^0), those helicity amplitudes are $\sim 1/E$, in agreement with the prediction of dimensional counting rules.

From the amplitudes thus obtained, one derives the transverse-momentum spectrum for the subprocess considered, taking account of kinematic factors (also restricted to order η^0), coupling constants, and the color factor:

$$\frac{d\sigma^{qg\rightarrow q'G}}{dp_T}(E,p_T) = \frac{\pi^2\alpha_s^3}{24E^3(E^2-4p_T^2)^{1/2}}\sum_{\lambda_q\lambda_g,\lambda_{q'}\Lambda}[\,|\mathcal{M}_{qg\rightarrow q'G}^{\lambda_q\lambda_g,\lambda_{q'}\Lambda}(E,\Theta)|^2+|\mathcal{M}_{qg\rightarrow q'G}^{\lambda_q\lambda_g,\lambda_{q'}\Lambda}(E,\pi-\Theta)|^2] , \tag{22}$$

where, in the expressions of the said amplitudes, $\cos\Theta$ is to be replaced by $(1-4p_T^2/E^2)^{1/2}$.

The transverse-momentum spectrum for the overall reaction $p\bar{p}\rightarrow qGX$ (see diagram (a) of Fig. 3) is then obtained by convoluting the spectrum given by formula (22) with the distribution functions of the quark and the gluon as follows:

$$\frac{d\sigma^{p\bar{p}\rightarrow q'GX}}{dp_T}(s,p_T) = 2\sum_q\int_{x_{\min}}^1 dx\int_{x'_{\min}}^1 dx'[f_{q/p}(x,``Q^2")+f_{\bar{q}/p}(x,``Q^2")]f_{g/p}(x',``Q^2")\frac{d\sigma^{qg\rightarrow q'G}}{dp_T}(E,p_T) , \tag{23}$$

where s is the total energy squared in the c.m. frame of the $p\bar{p}$ collision and where we have used the equalities $f_{q/\bar{p}}=f_{\bar{q}/p}$, $f_{\bar{q}/\bar{p}}=f_{q/p}$, and $f_{g/\bar{p}}=f_{g/p}$. The summation is over quark flavors $q=u,\,d,\,s$, and possibly c; actually we use (both for the quark and gluon distributions) the parametrization of Duke and Owens [12] that contains indeed a small contribution of c quarks. For the scale "Q^2", we choose "Q^2"$=M^2$. We note that $E^2=xx's$, and thus

$$x'_{\min}=\frac{E_{\min}^2}{xs}, \quad x=\frac{E_{\min}^2}{s} \quad \text{with } E_{\min}^2=4p_T^2 . \tag{24}$$

In order to eliminate from our results the unknown (or at least theoretically not well determined) parameters, i.e., the glueballs' radial wave functions (their derivatives) at the origin in configuration space, we proceed again as in Ref. [4]: We normalize those results with the help of the radiative decay widths of the J/ψ for the same glue-
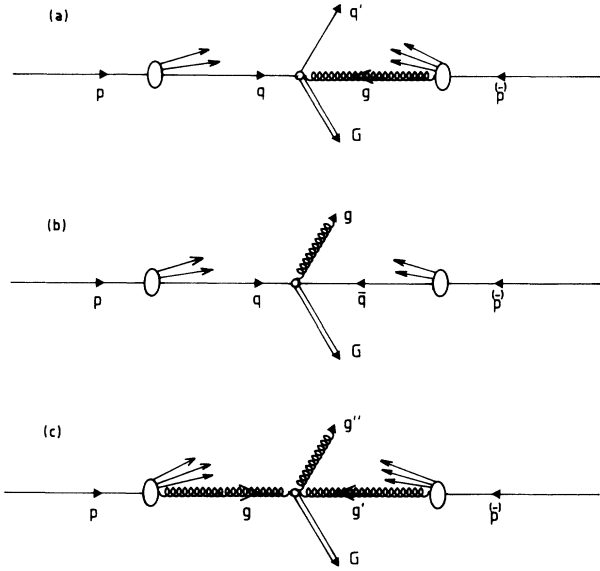
FIG. 3. Diagrams representing the contributions of the sub-processes (a) $qg \rightarrow q'G$, (b) $q\bar{q} \rightarrow gG$, and (c) $gg' \rightarrow g''G$ to the reaction $p\bar{p} \rightarrow$ jet $+ G + X$.

ball candidates and quantum states:

$$\frac{d\sigma^{p\bar{p} \rightarrow qGX}}{dp_T} B(G \rightarrow xy \cdots)$$

$$= \frac{d\sigma^{p\bar{p} \rightarrow qGX}}{dp_T} \frac{\Gamma(J/\psi \rightarrow \gamma G)B(G \rightarrow xy \cdots)}{\Gamma(J/\psi \rightarrow \gamma G)}, \quad (25)$$

where, in the second factor on the right-hand side, we take the numerator from the experimental literature (actually, we take the same values as in Ref. [4], since those values have not significantly changed after that paper was published), while analytic expressions of the denominator are to be taken, as well, from Ref. [4] (see [13]).

There is in principle no free parameter left in our results; however, a certain freedom of choice remains as regards α_s factors: We get a factor α_s^3 in the numerator from formula (22), while on the other hand the denominator $\Gamma(J/\psi \rightarrow \gamma G)$ contains a factor α_s^2. We here suppose that α_s keeps approximately the same value in both processes $qg \rightarrow q'G$ and $J/\psi \rightarrow \gamma G$, so that we are simply left with a factor α_s; as regards the latter, we assume that its expression is given by

$$\alpha_s = \alpha_s(M^2) = 12\pi/[25 \ln(M^2/\Lambda^2)] \quad \text{with} \quad \Lambda = 0.2 \ . \quad (26)$$

The p_T spectra thus obtained are shown, for the three glueball candidates and two machine energies considered (pertaining to the CERN $Sp\bar{p}S$ and the Fermilab Tevatron, respectively), in Figs. 4–9 (curves labeled "qg"). For simplicity we there exhibit our results only for one particular quantum state of either of the glueball candidates $f_2(1720)$ and $X(2220)$. The spectra obtained for other quantum states are, at order η^0, strictly proportional to those shown in the said figures; the corresponding proportionality coefficients are given in Table I.
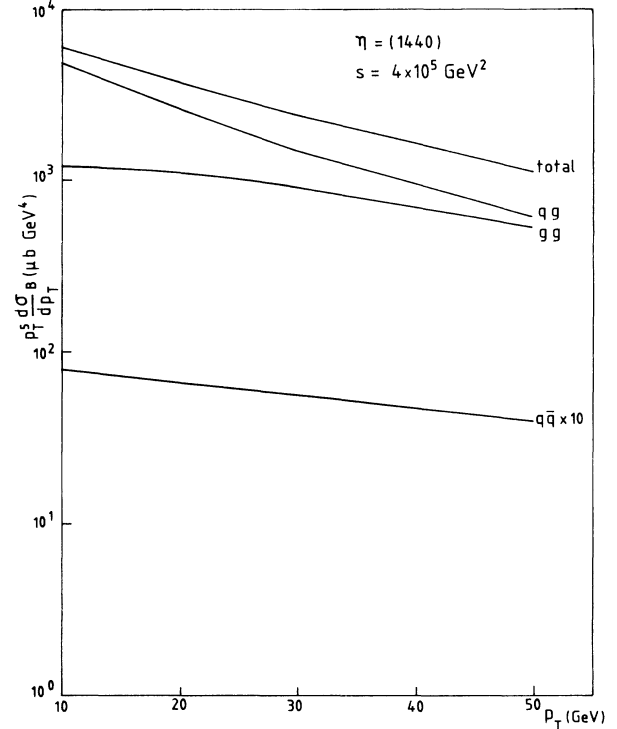
FIG. 4. Contributions of the various subprocesses ($qg \rightarrow qG$, $q\bar{q} \rightarrow gG$, $gg \rightarrow gG$) to the transverse-momentum spectrum, multiplied by p_T^5 and B, predicted for the reaction $p\bar{p} \rightarrow$ jet $+ G + X$, with $G = \eta(1440)$, at $s = 4 \times 10^5$ GeV^2; sum of those contributions. $B \equiv B(\eta(1440) \rightarrow K\bar{K}\pi)$.
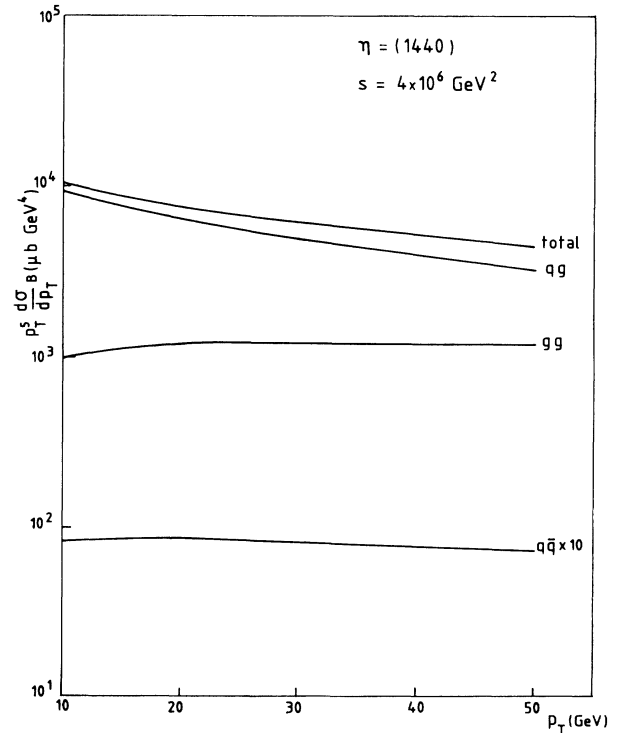
FIG. 5. Same as Fig. 4, at $s = 4 \times 10^6$ GeV^2.
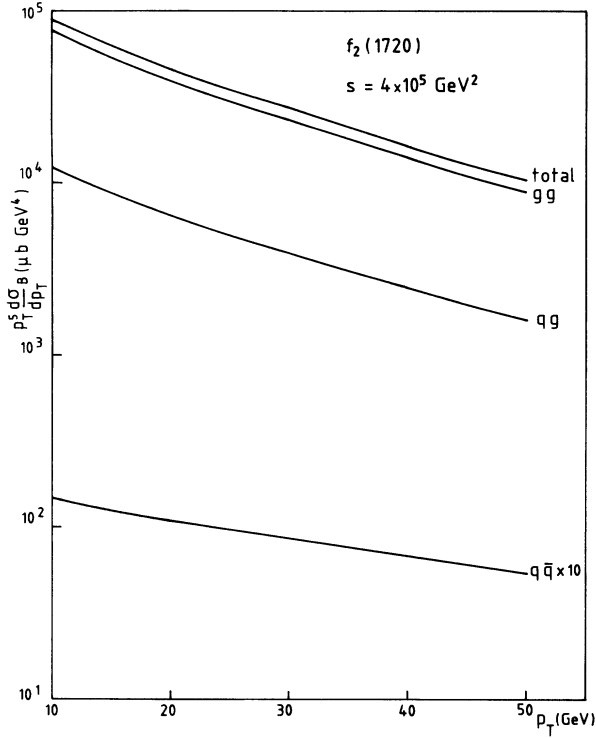
FIG. 6. Same as Fig. 4, with $G \equiv f_2(1740)$, $B \equiv B(f_2(1720) \rightarrow K\overline{K})$. The quantum state chosen for the $f_2(1720)$ is the one called "$L = m$" in Ref [4] (see [15]).
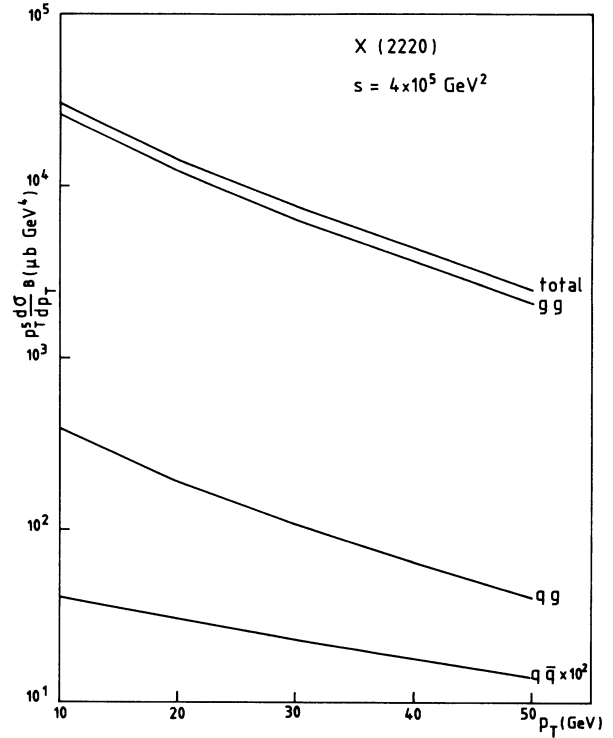
FIG. 8. Same as Fig. 4, with $G \equiv X(2220)$, $B \equiv B(X(2220) \rightarrow K\overline{K})$. The quantum state chosen for the $X(2220)$ is $J = 4$, $L = 2$.
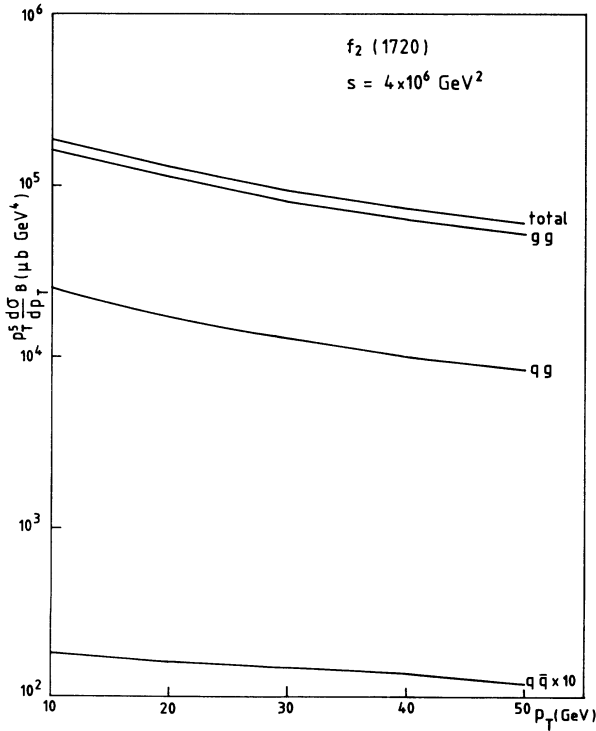
FIG. 7. Same as Fig. 6, at $s = 4 \times 10^6$ GeV^2.
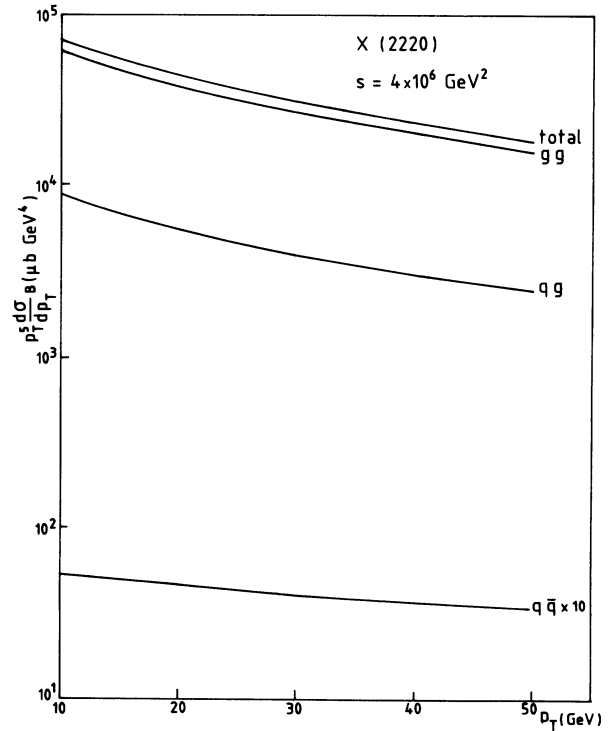
FIG. 9. Same as Fig. 8, at $s = 4 \times 10^6$ GeV^2.

TABLE I. Proportionality coefficients for various quantum states of $f_2(1720)$ and $X(2220)$, other than those considered in Figs. 7–10. These coefficients are, at order η^0, the same for the contributions of the different subprocesses and, of course, for their sum. The states called "$L=2$" and "$L=m$" for $f_2(1720)$ are the mixtures defined in Refs. [4,15].

$f_2(1720)$	$\dfrac{d\sigma/dp_T(L=0)}{d\sigma/dp_T(L=m)}=5.8\times10^{-2}$	
	$\dfrac{d\sigma/dp_T(L=2)}{d\sigma/dp_T(L=m)}=6.9\times10^{-1}$	
$X(2220)$	$\dfrac{d\sigma/dp_T(J=0,L=0)}{d\sigma/dp_T(J=4,L=2)}=3.3\times10^{-3}$	
	$\dfrac{d\sigma/dp_T(J=2,L=0)}{d\sigma/dp_T(J=4,L=2)}=1.9\times10^{-2}$	

Comments on these results, as well as on those of the following subsections, will be presented in Sec. IV.

B. Contribution of the subprocess $q\bar{q}\to gGX$

We might here apply a procedure completely analogous to that of Sec. III A, starting from the expressions of the helicity amplitudes for the Feynman graphs corresponding to this subprocess. However, we are able to proceed in a much simpler way, once we note that the subprocesses $qg\to q'G$ and $q\bar{q}\to gG$ are connected by crossing symmetry. Consequently, we may apply the "substitution law" well known from quantum electrodynamics [14], which allows us to derive directly the dynamic factor

$$\sum_{\lambda_q\lambda_{\bar{q}},\lambda_g\Lambda}|\mathcal{M}_{q\bar{q}\to gG}^{\lambda_q\lambda_{\bar{q}},\lambda_g\Lambda}(E,\Theta)|^2 \ ,$$

from the analytic expression obtained in Sec. III A for

$$\sum_{\lambda_q\lambda_g,\lambda'_q\Lambda}|\mathcal{M}_{qg\to q'G}^{\lambda_q\lambda_g,\lambda'_q\Lambda}(E,\Theta)|^2 \ ,$$

by making the substitution $\hat{s},\hat{t},\hat{u}\to\hat{t},\hat{s},\hat{u}$ (calling $\hat{s},\hat{t},\hat{u}$ the Mandelstam variables of either subprocess). More precisely, that means making the following substitutions (at order η^0):

$$E^2\to-\frac{E^2}{2}(1-\cos\Theta), \quad \cos\Theta\to-\frac{3+\cos\Theta}{1-\cos\Theta} \ . \tag{27}$$

In addition, the overall sign of the dynamic factor is to be changed. Therefore, taking account of kinematic factors, coupling constants, and the color factor, one gets

$$\frac{d\sigma^{q\bar{q}\to gG}}{dp_T}(E,p_T)=\frac{\pi^2\alpha_s^3}{9E^3(E^2-4p_T^2)^{1/2}}\sum_{\lambda_q\lambda_{\bar{q}},\lambda_g\Lambda}[\,|\mathcal{M}_{q\bar{q}\to gG}^{\lambda_q\lambda_{\bar{q}},\lambda_g\Lambda}(E,\Theta)|^2+|\mathcal{M}_{q\bar{q}\to gG}^{\lambda_q\lambda_{\bar{q}},\lambda_g\Lambda}(E,\pi-\Theta)|^2] \ , \tag{28}$$

where $\cos\Theta$ is to be replaced by $(1-4p_T^2/E^2)^{1/2}$.

The next step is deriving the transverse-momentum spectrum for the contribution of the subprocess considered to the overall reaction $p\bar{p}\to gGX$ [see diagram (b) of Fig. 3] by performing the convolution

$$\left[\frac{d\sigma^{p\bar{p}\to gGX}}{dp_T}(s,p_T)\right]_{q\bar{q}}$$

$$=\sum_q\int_{x_{\min}}^1 dx\int_{x'_{\min}}^1 dx'[f_{q/p}(x,"Q^2")f_{q/p}(x',"Q^2")+f_{\bar{q}/p}(x,"Q^2")f_{\bar{q}/p}(x',"Q^2")]\frac{d\sigma^{q\bar{q}\to gG}}{dp_T}(E,p_T) \ . \tag{29}$$

Here again we choose "Q^2"$=M^2$ and use the parametrization of Ref. [12] for the distribution functions. The limits of integration are again given by (27). The last step consists in normalizing our results as in Sec. III A:

$$\left[\frac{d\sigma^{p\bar{p}\to gGX}}{dp_T}\right]_{q\bar{q}}B(G\to xy\cdots)=\left[\frac{d\sigma^{p\bar{p}\to gGX}}{dp_T}\right]_{q\bar{q}}\frac{\Gamma(J/\psi\to\gamma G)B(G\to xy\cdots)}{\Gamma(J/\psi\to\gamma G)} \ , \tag{30}$$

using the same conventions as defined after formula (28).

The corresponding results are shown in Figs. 4–9 (curves labeled "$q\bar{q}$") for the two machine energies considered and the quantum states retained. Proportionality coefficients for other quantum states are, at order η^0, the same as for the subprocess $qg\to q'G$ and are thus to be found as well in Table I.

C. Contribution of the subprocess $gg'\to g''g_1g_2$

Here we compute the graphs (1)–(12) of Fig. 10. The contribution of each graph, except for (9), (10), and (12), is doubled when we take account of the exchange $g_1\leftrightarrow g_2$. Here again we call all four-momenta like the corresponding particles, i.e., g,g',g'',g_1,g_2, and we associate with those particles their respective polarization four-vectors ε^λ, $\varepsilon'^{\lambda'},\varepsilon''^{\lambda''},\varepsilon_1^{\lambda_1},\varepsilon_2^{\lambda_2}$. In the following expressions of the helicity amplitudes for the individual graphs, we leave aside the coupling constants, as well as a common color factor $1/(2\sqrt{2})f_{abc}$ (where f_{abc} are the antisymmetric structure constants of the group of Gell-Mann matrices [11], calling a,b,c the color indices of the gluons g,g',g''). We get
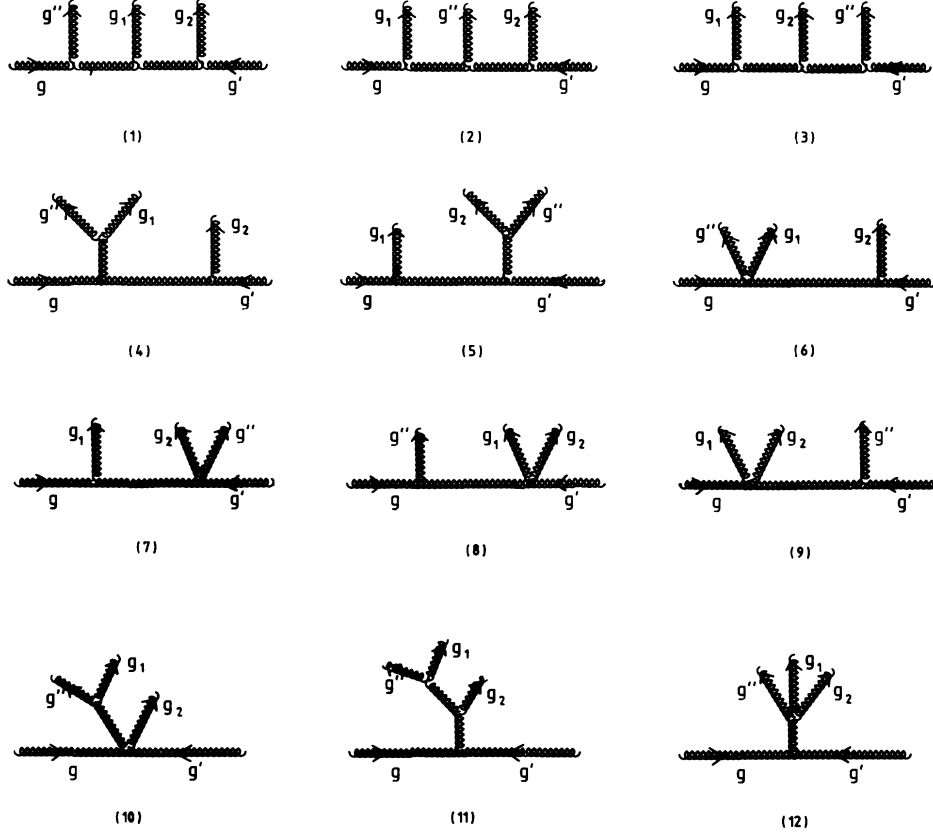
FIG. 10. Feynman graphs for the subprocess $gg' \to g''g_1g_2$. Other graphs, providing the same contribution to the helicity amplitudes of the subprocess $gg' \to g''G$, are derived from those here represented (except for graphs 8, 9, and 12) by exchanging g_1 and g_2.

$$\mathcal{M}_{(1)}^{\lambda\lambda',\lambda''\lambda_1\lambda_2} = -3[(\varepsilon^{\lambda}\cdot\varepsilon''^{*\lambda''})(g+g'')_\mu - 2(g\cdot\varepsilon''^{*\lambda''})\varepsilon_\mu^{\lambda} - 2(g''\cdot\varepsilon^{\lambda})\varepsilon_\mu''^{*\lambda''}]$$

$$\times[\varepsilon_1^{*\lambda_1^\mu}(g-g''+g_1)^\nu - 2(g-g'')\cdot\varepsilon_1^{*\lambda_1}g^{\mu\nu} + (g-g''-2g_1)^\mu\varepsilon_1^{*\lambda_1^\nu}]$$

$$\times[2(g_2\cdot\varepsilon'^{\lambda'})\varepsilon_{2\nu}^{*\lambda_2} + 2(g'\cdot\varepsilon_2^{*\lambda_2})\varepsilon_\nu'^{\lambda'} - (\varepsilon'^{\lambda'}\cdot\varepsilon_2^{*\lambda_2})(g'+g_2)_\nu]\cdot(g-g'')^{-2}(g'-g_2)^{-2} , \tag{31}$$

$$\mathcal{M}_{(2)}^{\lambda\lambda',\lambda''\lambda_1\lambda_2} = -3[(\varepsilon^{\lambda}\cdot\varepsilon_1^{*\lambda_1})(g+g_1)_\mu - 2(g\cdot\varepsilon_1^{*\lambda_1})\varepsilon_\mu^{\lambda} - 2(g_1\cdot\varepsilon^{\lambda})\varepsilon_{1\mu}^{*\lambda_1}]$$

$$\times[\varepsilon''^{*\lambda''^\mu}(g+g''-g_1)^\nu - 2(g-g_1)\cdot\varepsilon''^{*\lambda''}g^{\mu\nu} + (g-2g''-g_1)^\mu\varepsilon''^{*\lambda''^\nu}]$$

$$\times[2(g'\cdot\varepsilon_2^{*\lambda_2})\varepsilon_\nu'^{\lambda'} - 2(\varepsilon'^{\lambda'}\cdot\varepsilon_2^{*\lambda_2})(g'+g_2)_\nu + 2(g_2\cdot\varepsilon'^{\lambda'})\varepsilon_{2\nu}^{*\lambda_2}]\cdot(g-g_1)^{-2}(g'-g_2)^{-2} , \tag{32}$$

$$\mathcal{M}_{(3)}^{\lambda\lambda',\lambda''\lambda_1\lambda_2} = -\mathcal{M}_{(1)}^{\lambda\lambda',\lambda''\lambda_1\lambda_2}(g\leftrightarrow g', \varepsilon^{\lambda}\leftrightarrow\varepsilon'^{\lambda'}, g_1\leftrightarrow g_2, \varepsilon_1^{\lambda_1}\leftrightarrow\varepsilon_2^{\lambda_2}) , \tag{33}$$

$$\mathcal{M}_{(4)}^{\lambda\lambda',\lambda''\lambda_1\lambda_2} = -\tfrac{3}{2}[(\varepsilon''^{*\lambda''}\cdot\varepsilon_1^{*\lambda_1})(g_1-g'')_\mu + 2(g''\cdot\varepsilon_1^{*\lambda_1})\varepsilon_\mu''^{*\lambda''} - 2(g_1\cdot\varepsilon''^{*\lambda''})\varepsilon_{1\mu}^{*\lambda_1}]$$

$$\times[\varepsilon^{\lambda\mu}(g+g''+g_1)^\nu - (2g-g''-g_1)^\mu\varepsilon^{\lambda\nu} - 2(g''+g_1)\cdot\varepsilon^{\lambda}g^{\mu\nu}]$$

$$\times[2(g'\cdot\varepsilon_2^{*\lambda_2})\varepsilon_\nu'^{\lambda'} - 2(\varepsilon'^{\lambda'}\cdot\varepsilon_2^{*\lambda_2})(g'+g_2)_\nu + 2(g_2\cdot\varepsilon'^{\lambda'})\varepsilon_{2\nu}^{*\lambda_2}]\cdot(g''+g_1)^{-2}(g'-g_2)^{-2} , \tag{34}$$

$$\mathcal{M}_{(5)}^{\lambda\lambda',\lambda''\lambda_1\lambda_2} = -\mathcal{M}_{(4)}^{\lambda\lambda',\lambda''\lambda_1\lambda_2}(g\leftrightarrow g', \varepsilon^{\lambda}\leftrightarrow\varepsilon'^{\lambda'}, g_1\leftrightarrow g_2, \varepsilon_1^{\lambda_1}\leftrightarrow\varepsilon_2^{\lambda_2}) , \tag{35}$$

$$\mathcal{M}_{(6)}^{\lambda\lambda',\lambda''\lambda_1\lambda_2} = \tfrac{9}{2}[(\varepsilon^{\lambda}\cdot\varepsilon_1^{\lambda_1})\varepsilon_\mu''^{*\lambda''} - (\varepsilon''^{*\lambda''}\cdot\varepsilon_1^{\lambda_1})\varepsilon_\mu^{\lambda}][2(g_2\cdot\varepsilon^{\lambda})\varepsilon_2^{*\lambda_2^\mu} + 2(g''\cdot\varepsilon_2^{*\lambda_2})\varepsilon'^{\lambda'\mu} - (\varepsilon'^{\lambda'}\cdot\varepsilon_2^{*\lambda_2})(g'+g_2)^\mu]\cdot(g'-g_2)^{-2} , \tag{36}$$

$$\mathcal{M}_{(7)}^{\lambda\lambda',\lambda''\lambda_1\lambda_2} = -\mathcal{M}_{(6)}^{\lambda\lambda',\lambda''\lambda_1\lambda_2}(g\leftrightarrow g', \varepsilon^{\lambda}\leftrightarrow\varepsilon'^{\lambda'}, g_1\leftrightarrow g_2, \varepsilon_1^{\lambda_1}\leftrightarrow\varepsilon_2^{\lambda_2}) , \tag{37}$$

$$\mathcal{M}_{(8)}^{\lambda\lambda',\lambda''\lambda_1\lambda_2} = -3[(\varepsilon''^{*\lambda''}\cdot\varepsilon^{\lambda})(g+g'')_\mu - 2(g\cdot\varepsilon''^{*\lambda''})\varepsilon_\mu^{\lambda} - 2(g''\cdot\varepsilon^{\lambda})\varepsilon_\mu''^{*\lambda''}]$$

$$\times[(\varepsilon'^{\lambda'}\cdot\varepsilon_1^{*\lambda_1})\varepsilon_2^{*\lambda_2^\mu} + (\varepsilon'^{\lambda'}\cdot\varepsilon_2^{*\lambda_2})\varepsilon_1^{*\lambda_1^\mu} - 2(\varepsilon_1^{*\lambda_1}\cdot\varepsilon_2^{*\lambda_2})\varepsilon'^{\lambda'\mu}](g-g'')^{-2} , \tag{38}$$

$$\mathcal{M}_{(9)}^{\lambda\lambda',\lambda''\lambda_1\lambda_2} = -\mathcal{M}_{(8)}^{\lambda\lambda',\lambda''\lambda_1\lambda_2}(g\leftrightarrow g', \varepsilon^\lambda\leftrightarrow\varepsilon'^{\lambda'}) , \tag{39}$$

$$\mathcal{M}_{(10)}^{\lambda\lambda',\lambda''\lambda_1\lambda_2} = -\tfrac{9}{2}[(\varepsilon''^{*\lambda''}\cdot\varepsilon_1^{*\lambda_1})(g_1-g'')_\mu+2(g''\cdot\varepsilon_1^{*\lambda_1})\varepsilon_\mu''^{*\lambda''}-2(g_1\cdot\varepsilon_\mu''^{*\lambda''})\varepsilon_{1\mu}^{*\lambda_1}][(\varepsilon^\lambda\cdot\varepsilon_2^{*\lambda_2})\varepsilon'^{\lambda'\mu}-(\varepsilon'^{\lambda'}\cdot\varepsilon_2^{*\lambda_2})\varepsilon^{\lambda\mu}](g''+g_1)^{-2} , \tag{40}$$

$$\mathcal{M}_{(11)}^{\lambda\lambda',\lambda''\lambda_1\lambda_2} = 3[(\varepsilon''^{*\lambda''}\cdot\varepsilon_1^{*\lambda_1})(g''-g_1)_\mu-2(g'\cdot\varepsilon_1^{*\lambda_1})\varepsilon_\mu''^{*\lambda''}+2(g_1\cdot\varepsilon''^{*\lambda''})\varepsilon_{1\mu}^{*\lambda_1}]$$

$$\times[\varepsilon_2^{*\lambda_2^\mu}(g_2-g''-g_1)^\nu-(g''+g_1+2g_2)^\mu\varepsilon_2^{*\lambda_2^\nu}+2(g''+g_1)\cdot\varepsilon_2^{*\lambda_2}g^{\mu\nu}]$$

$$\times[2(g\cdot\varepsilon'^{\lambda'})\varepsilon_\nu^\lambda-(\varepsilon'^{\lambda'}\cdot\varepsilon^\lambda)(g-g')_\nu-2(g'\cdot\varepsilon^\lambda)\varepsilon_\nu'^{\lambda'}]\cdot(g''+g_1)^{-2}(g+g')^{-2} , \tag{41}$$

$$\mathcal{M}_{(12)}^{\lambda\lambda',\lambda''\lambda_1\lambda_2} = 3[2(\varepsilon_1^{*\lambda_1}\cdot\varepsilon_2^{*\lambda_2})\varepsilon_\mu''^{*\lambda''}-(\varepsilon^{*\lambda''}\cdot\varepsilon^{*\lambda_2})\varepsilon_{1\mu}^{*\lambda_1}-(\varepsilon''^{*\lambda''}\cdot\varepsilon_1^{*\lambda_1})\varepsilon_{2\mu}^{*\lambda_2}]$$

$$\times[2(g\cdot\varepsilon'^{\lambda'})\varepsilon^{\lambda\mu}-(\varepsilon^\lambda\cdot\varepsilon'^{\lambda'})(g-g')^\mu-2(g'\cdot\varepsilon^\lambda)\varepsilon'^{\lambda'\mu}](g+g')^{-2} . \tag{42}$$

Summing up those amplitudes and applying formula (11), we are led to the helicity amplitudes $\mathcal{M}_{gg'\to g''G}^{\lambda\lambda',\lambda''\Lambda}$ that are given in Appendix B for the various glueball quantum states considered. Therefrom, taking account of kinematic factors, coupling constants, and the color factor, we get

$$\frac{d\sigma^{gg'\to g''G}}{dp_T}(E,p_T) = \frac{3\pi^2\alpha_s^3}{128E^3(E^2-4p_T^2)^{1/2}}\sum_{\lambda\lambda',\lambda''\Lambda}[|\mathcal{M}_{gg'\to g''G}^{\lambda\lambda',\lambda''\Lambda}(E,\Theta)|^2+|\mathcal{M}_{gg'\to g''G}^{\lambda\lambda',\lambda''\Lambda}(E,\pi-\Theta)|^2] , \tag{43}$$

where $\cos\Theta$ is to be replaced by $(1-4p_T^2/E^2)^{1/2}$.

The next step is computing the contribution of that subprocess to the overall reaction $p\bar{p}\to gG$ [see Fig. 3(c)] by convoluting the above transverse-momentum spectrum with the gluon distribution functions:

$$\left[\frac{d\sigma^{p\bar{p}\to g''GX}}{dp_T}(s,p_T)\right]_{gg'} = \int_{x_{min}}^1 dx \int_{x'_{min}}^1 dx' f_{g/p}(x,\text{``}Q^{2\text{''}})f_{g/p}(x',\text{``}Q^{2\text{''}})\frac{d\sigma^{gg'\to g''G}}{dp_T}(E,p_T) , \tag{44}$$

where again we use the parametrization of Ref. [12], taking "Q^2"$=M^2$. The limits of integration are again given by (24). Once more we normalize our results with the help of the data and analytic results regarding radiative J/ψ decay:

$$\left[\frac{d\sigma^{p\bar{p}\to gGX}}{dp_T}\right]_{gg} B(G\to xy\cdots) = \left[\frac{d\sigma^{p\bar{p}\to gGX}}{dp_T}\right]_{gg}\frac{\Gamma(J/\psi\to\gamma G)B(G\to xy\cdots)}{\Gamma(J/\psi\to\gamma G)} , \tag{45}$$

and using the same conventions as in Sec. III A, we thus obtain the p_T spectra shown in Figs. 4–9 (curves labeled "gg") for the two machine energies considered and the quantum states retained. Proportionality coefficients for other quantum states are again the same as for the previous subprocesses and are thus to be found in Table I.

D. Total result

We assume that, from an experimental point of view, it might be difficult to differentiate between quark and gluon jets; therefore, we sum up the contributions of all three subprocesses in order to evaluate the p_T spectra for the overall reaction $p\bar{p}\to\text{jet}+\text{glueball}+X$. Those spectra are shown in Figs. 4–9 for the two machine energies considered and for the quantum states selected; for other quantum states, the proportionality coefficients to be used are, again, those given in Table I. All comments are left for Sec. IV.

IV. DISCUSSION AND CONCLUSION

Before we analyze our results, let us remark that there are various sources of uncertainty to be considered (apart from the fact that the validity of our model, as of any other phenomenological model, may be questioned).

(i) We have checked the validity of the approximation used, i.e, keeping only the lowest-order term in the series expansion in powers of $\eta=M/E$, by including in our computations the next-order correction, i.e., terms up to order η^2 in the differential cross section $d\sigma/dp_T$; the modification thus induced in our results does not exceed 10%.

(ii) Some doubt may arise as regards the parametrization used for the quark and gluon distribution functions because of the fact that very small values of the scaling variables are involved. Indeed, one notes that $x_{min}=x'_{min}=10^{-3}$ at $p_T=10$ GeV and $s=4\times10^5$ GeV^2 and that this value goes down to 10^{-4} at $p_T=10$ GeV and $s=4\times10^6$ GeV^2. It is well known that in that range the distribution functions have not been accurately checked by experimental measurements until now. Let us simply mention that, in addition to the parametrization of Ref. [12], we have tried an alternative one [16] and the latter gives rise systematically to somewhat higher predictions (by a factor of about 3–4).

(iii) The choice of the scale "Q^2"$=M^2$ in the expressions of the distribution functions may appear questionable. Therefore, we have performed, alternatively, a calculation with "Q^2"$=p_T^2$; we noted that, while our predictions would thus be systematically increased, they would not change by more than 30%.

(iv) Restricting ourselves to computing lowest-order Feynman diagrams in QCD should not entail too large an error, since α_s is relatively small with respect to 1 (with our choice, $\alpha_s \simeq 0.3 - 0.35$).

(v) Finally, the largest possible source of error proceeds from our choice of the value of α_s. A different choice, e.g., $\alpha_s \simeq 0.2$, might result in decreasing our results substantially, but not by more than one order of magnitude.

This being said, the analysis of our results leads us to the following conclusions.

(a) Roughly speaking, the p_T spectra obtained tend to decrease like p_T^{-5}, in agreement with the prediction of dimensional counting rules; actually, the decrease is generally somewhat faster because of logarithmic factors appearing when one passes from the parton to the hadron cross section (more precisely when one integrates the parton cross section, convoluted with the parton distribution functions, over x, x').

(b) Correspondingly, it is only through those logarithmic factors (of the type $\ln s / (4p_T^2)$ [$\ln^2 s / (4p_T^2)$]) that the p_T spectra depend on s, i.e., on the machine energy; it results that there is a slight increase, accompanied by a flattening of the curves, when one passes from $S p\bar{p} S$ to Tevatron energy.

(c) It appears from Figs. 4–9 and Table I that, for a given machine energy and hard-collision subprocess, all curves obtained for different glueball candidates and quantum states considered [except in some cases for the pseudoscalar $\eta(1440)$] are parallel or almost parallel to each other. Obviously, this is mainly due to the fact that we are allowed to keep only terms of order η^0 (see the expressions of the helicity amplitudes in the Appendixes).

(d) The contribution of the reaction mechanism $q\bar{q}$ is systematically negligible (it therefrom results that the total result would practically be the same for a pp instead of a $p\bar{p}$ collider). As regards the two other subprocesses, the contribution of $gg \rightarrow gG$ is dominating, for the $f_2(1720)$ and the $X(2220)$, over that of $qg \rightarrow qG$; on the other hand, the inverse is true for the $\eta(1440)$.

(e) If one integrates the spectra obtained over p_T, assuming $p_{T_{\min}} = 10$ GeV and an ideal experimental situation where there are no other acceptance cuts, the integrated cross sections predicted are (taking into account the above-made remarks regarding uncertainties of our results) of the order of $10^{-33} - 10^{-30}$ cm^2, depending on the glueball candidate and quantum state considered.

We thus conclude that one may expect an abundant production of glueball candidates in high-energy hadronic collisions to be performed with presently available colliders. The main problem, however, will be the separation of this signal from the background due to production of two jets (mainly gluon jets), with one of them involving low particle multiplicity. A study performed by Lutz [17], using the data collected by the DELPHI Collaboration at the CERN e^+e^- collider LEP in 1990, regarding multiplicity and invariant-mass distributions of gluon jets emitted at large transverse momentum (in particular in the range 10 GeV/$c < p_T < 20$ GeV/c), allows us to draw some rough conclusions as to the signal/background ratio to be expected. Assuming our results shown in Figs.

4–9 to be valid, considering the most favorable decay channel for each glueball candidate [i.e., $K^+ K^- \pi^0$ for $\eta(1440)$ and $K^+ K^-$ for both $f_2(1720)$ and $X(2220)$], and assuming in addition that the three- or two-particle invariant mass is measured with a precision of ± 100 MeV, we conclude that the signal/background ratio should be relatively large (≈ 10) for $f_2(1720)$, slightly smaller for $X(2220)$, and somewhat less than 1 for $\eta(1440)$. Actually, these ratios might be improved by about one order of magnitude if a good experimental discrimination is performed between charged kaons and pions.

However, these conclusions should not be taken at face value, given our uncertainty regarding the quantum state of the candidates $f_2(1720)$ and $X(2220)$ and, in addition, various factors of uncertainty mentioned in the beginning of this section. Moreover, our implicit assumption that gluon jets in a given p_T range are fragmenting in the same way whatever their origin ($p\bar{p}$ or e^+e^- collisions) might not be absolutely valid.

It should also be emphasized that, given the different p_T behavior of the signal (p_T^{-5}) and the background (p_T^{-3}), their ratio critically depends on the minimal value of the transverse momentum measured; i.e, a smaller $p_{T_{\min}}$ will improve the chances of identifying glueball candidates in the process here studied, while a larger $p_{T_{\min}}$ might jeopardize them.

The model here used may allow one, in the future, to provide theoretical predictions as well for other processes that may be studied experimentally in the same context, e.g., $p\bar{p} \rightarrow GGX$ or $p\bar{p} \rightarrow GMX$, where M is an ordinary ($q\bar{q}$) meson. More generally, we think that this model, which is fit to be applied to quarkonia as well as gluonia, might provide an efficient tool for studies in meson spectroscopy.

Incidentally, let us mention that we have applied our model, in addition, to reactions of the type $pe \rightarrow qGX(e)$ (taking place via the subprocess $q\gamma \rightarrow q'G$) and $p\bar{p} \rightarrow \gamma GX$ (involving the subprocess $q\bar{q} \rightarrow \gamma G$), but the integrated cross sections obtained in both cases ($10^{-42} - 10^{-38}$ and $10^{-41} - 10^{-37}$ cm^2, respectively) appear too small to justify an experimental measurement.

The computer program REDUCE has been used extensively for our analytic computations.

APPENDIX A: HELICITY AMPLITUDES FOR THE PROCESS $qg \rightarrow q'G$

We shall here present the expressions of the helicity amplitudes $\mathcal{M}^{\lambda_q \lambda_g, \lambda_{q'} \Lambda}$ [18] obtained in our model (see Sec. III A) for the process $qg \rightarrow q'G$ at order η^0. We shall fix $\lambda_q = \lambda_{q'} = +\frac{1}{2}$, since those amplitudes are zero (for massless quarks) when $\lambda_q \neq \lambda_{q'}$ and since, on the other hand,

TABLE II. Expressions of the helicity amplitudes $\mathcal{M}^{\lambda_q \lambda_{q'};\lambda'_q \Lambda}$, with $\lambda_q = \lambda'_q = +\frac{1}{2}$, of the subprocess $qg \to q'G$ at order η^0 (see Appendix A for the definition of X and B_L). All other helicity amplitudes, for the quantum states (J,L,S) considered, are vanishing at that order.

	$\lambda_g = 1$	$\lambda_g = -1$
$J=0,\ L=S=1$	$-\frac{2}{3}i(8-16\bar{c}^2+35\bar{c}^4)B_1$	$-2i(8-7\bar{c}^2+8\bar{c}^4)\bar{c}^2 B_1$
$J=L=S=0$	$\frac{\sqrt{2}}{3\sqrt{3}}XB_0$	$-\frac{\sqrt{2}}{3\sqrt{3}}X\bar{c}^2 B_0$
$\Lambda=0$ $J=S=2,\ L=0$	$\frac{1}{3\sqrt{3}}XB_0$	$-\frac{1}{3\sqrt{3}}X\bar{c}^2 B_0$
$\Lambda=-2\lambda_g$	$-\frac{2\sqrt{2}}{3}XB_0$	$\frac{2\sqrt{2}}{3}X\bar{c}^2 B_0$
$\Lambda=0$ $J=L=2=S=0$	$-\frac{4\sqrt{10}}{\sqrt{3}}XB_2$	$\frac{4\sqrt{10}}{\sqrt{3}}X\bar{c}^2 B_2$
$\Lambda=-2\lambda_g$	$\frac{16\sqrt{5}}{3}XB_2$	$-\frac{16\sqrt{5}}{3}X\bar{c}^2 B_2$
$\Lambda=0$ $J=L=S=2$	$-\left(\frac{30}{7}\right)^{1/2}XB_2$	$\left(\frac{30}{7}\right)^{1/2}X\bar{c}^2 B_2$
$\Lambda=-2\lambda_g$	$\frac{4\sqrt{5}}{3\sqrt{7}}XB_2$	$-\frac{4\sqrt{5}}{3\sqrt{7}}X\bar{c}^2 B_2$
$\Lambda=0$ $J=4,\ L=S=2$	$-\frac{4\sqrt{6}}{\sqrt{7}}XB_2$	$\frac{4\sqrt{6}}{7}X\bar{c}^2 B_2$
$\Lambda=-2\lambda_g$	$-\frac{16\sqrt{5}}{\sqrt{21}}XB_2$	$\frac{16\sqrt{5}}{\sqrt{21}}X\bar{c}^2 B_2$

TABLE III. Expressions of the helicity amplitudes $\mathcal{M}^{\lambda\lambda',\lambda''\Lambda}$, with $\lambda=+1$, of the subprocess $gg' \to g''G$ at order η^0 (see Appendix B for the definition of Y and C_L). All other helicity amplitudes, for the quantum states (J,L,S) considered, are vanishing at that order.

	$\lambda'=\lambda''=1$	$\lambda'=-\lambda''=1$	$\lambda'=-\lambda''=-1$	$\lambda'=\lambda''=-1$
$J=0,\ L=S=1$	0	0	$-24i\bar{s}^2\bar{c}^2 C_1$	$24i\bar{s}^2\bar{c}^2 C_1$
$J=L=S=0$	$\sqrt{6}YC_0$	0	$-\sqrt{6}Y\bar{c}^2 C_0$	$\sqrt{6}Y\bar{s}^2 C_0$
$\Lambda=0$ $J=S=2,\ L=0$	$\sqrt{3}YC_0$	0	$-\sqrt{3}Y\bar{c}^2 C_0$	$\sqrt{3}Y\bar{s}^2 C_0$
$\Lambda=2\lambda''$	0	$-6\sqrt{2}YC_0$	$6\sqrt{2}Y\bar{c}^2 C_0$	$-6\sqrt{2}Y\bar{s}^2 C_0$
$\Lambda=0$ $J=L=2,\ S=0$	$-12\sqrt{30}YC_2$	0	$12\sqrt{30}Y\bar{c}^2 C_2$	$-12\sqrt{30}Y\bar{s}^2 C_2$
$\Lambda=2\lambda''$	0	$48\sqrt{5}YC_2$	$-48\sqrt{5}Y\bar{c}^2 C_2$	$48\sqrt{5}Y\bar{s}^2 C_2$
$\Lambda=0$ $J=L=S=2$	$-q\left(\frac{30}{7}\right)^{1/2}YC_2$	0	$9\left(\frac{30}{7}\right)^{1/2}Y\bar{c}^2 C_2$	$-9\left(\frac{30}{7}\right)^{1/2}Y\bar{s}^2 C_2$
$\Lambda=2\lambda''$	0	$12\left(\frac{5}{7}\right)^{1/2}YC_2$	$-12\left(\frac{5}{7}\right)^{1/2}Y\bar{c}^2 C_2$	$12\left(\frac{5}{7}\right)^{1/2}Y\bar{s}^2 C_2$
$\Lambda=0$ $J=4,\ L=S=2$	$-36\left(\frac{6}{7}\right)^{1/2}YC_2$	0	$36\left(\frac{6}{7}\right)^{1/2}Y\bar{c}^2 C_2$	$-36\left(\frac{6}{7}\right)^{1/2}Y\bar{s}^2 C_2$
$\Lambda=2\lambda''$	0	$-48\left(\frac{15}{7}\right)^{1/2}YC_2$	$48\left(\frac{15}{7}\right)^{1/2}Y\bar{c}^2 C_2$	$-48\left(\frac{15}{7}\right)^{1/2}Y\bar{s}^2 C_2$

one derives them for the case $\lambda_q = \lambda'_q = -\frac{1}{2}$ by applying the relation

$$\mathcal{M}^{-\lambda_q - \lambda'_g, -\lambda'_q - \Lambda} = (-1)^{J + L - \Lambda - 1} \mathcal{M}^{\lambda_q \lambda_g, \lambda'_q \Lambda} \ .$$

It results that the only helicity parameters on which those amplitudes depend are λ_g and Λ.

It is convenient to set

$$B_L = \left[\frac{1}{\pi} \right]^{1/2} \frac{1}{M^{L + 1/2}} \left[\left[\frac{d}{dr} \right]^L R_L(r) \right]_{r=0} \frac{1}{E \bar{s}^3 \bar{c}^2}$$

and

$$X = 4 + \bar{c}^2 + 4\bar{c}^4 \ ,$$

recalling $\bar{c} = \cos\Theta/2$, $\bar{s} = \sin\Theta/2$.

For the various quantum states considered, all amplitudes that are not vanishing at order η^0 are given in Table II.

APPENDIX B: HELICITY AMPLITUDES FOR THE PROCESS $gg' \to g''G$

We shall here give the expressions of the helicity amplitudes $\mathcal{M}^{\lambda\lambda', \lambda''\Lambda}$ obtained in our model (see Sec. III C) for the process $gg' \to g''G$ at order η^0. We shall fix $\lambda = +1$, since one can derive the amplitudes for $\lambda = -1$ by applying the relation

$$\mathcal{M}^{-\lambda - \lambda', -\lambda'' - \Lambda} = (-1)^{J + L - \Lambda - 1} \mathcal{M}^{\lambda\lambda', \lambda''\Lambda} \ .$$

Thus the only helicity parameters on which those amplitudes depend are λ', λ'', and Λ.

It is convenient to set

$$\mathcal{C}_L = \left[\frac{1}{\pi} \right]^{1/2} \frac{1}{\mathcal{M}^{L + 1/2}} \left[\left[\frac{d}{dr} \right]^L R_L(r) \right]_{r=0} \frac{1}{\bar{s}^3 \bar{c}^3}$$

and $Y = 1 - \bar{c}^2 + \bar{c}^4$.

For the various quantum states considered, all helicity amplitudes that are not vanishing at order η^0 are given in Table III.

[1] H. Fritzsch and M. Gell-Mann, in *Proceedings of the XVIth International Conference on High-Energy Physics*, Chicago, Illinois 1972, edited by J. S. Jackson and A. Roberts (NAL, Batavia, 1973), Vol. 2, p. 135.

[2] For an experimental review, see, e.g., A. Palano, Report No. CERN-EP/87-92, 1987 (unpublished).

[3] M. Benayoun, Ph. Leruste, J. L. Narjoux, and R. Petronzio, Nucl. Phys. **B282**, 653 (1987); see also the experimental study presented by M. Benayoun et al., Phys. Lett. B **198**, 281 (1987).

[4] E. H. Kada, P. Kessler, and J. Parisi, Phys. Rev. D **39**, 2657 (1989).

[5] J. H. Kühn, J. Kaplan, and E. G. O. Safiani, Nucl. Phys. **B157**, 125 (1979); B. Guberina, J. H. Kühn, R. D. Peccei, and R. Rückl, *ibid.* **B174**, 137 (1980).

[6] R. N. Cahn, Phys. Rev. D **35**, 3342 (1987).

[7] See, e.g., D. M. Brink and G. R. Satchler, *Angular Momentum* (Clarendon, Oxford, 1962).

[8] See M. E. Rose, *Elementary Theory of Angular Momentum* (Wiley, New York, 1957).

[9] G. P. Lepage and S. J. Brodsky, Phys. Rev. D **22**, 2157 (1980); S. J. Brodsky and G. P. Lepage, *ibid.* **24**, 1808 (1981); **24**, 2948 (1981).

[10] M. Benayoun and M. Froissart, Nucl. Phys. **B315**, 295 (1989).

[11] M. Gell-Mann, Phys. Rev. **125**, 1067 (1962). Regarding the computation of color factors in QCD Feynman diagrams, see, e.g., R. Cutler and D. Sivers, Phys. Rev. D **17**, 196 (1978), Appendix B.

[12] D. W. Duke and J. F. Owens, Phys. Rev. D **30**, 49 (1984).

[13] We have systematically multiplied those decay widths by a factor of 4, because in Ref. [4] the helicity amplitudes of the process $J/\psi \to \gamma G$ had been underestimated by a factor of 2. On the other hand, we have corrected two misprints that appeared in Ref. [4], regarding the widths of J/ψ radiative decay into glueballs with quantum states $J = 0$, $L = S = 1$ and $J = 4$, $L = S = 2$.

[14] See J. M. Jauch and F. Rohrlich, *The Theory of Photons and Electrons* (Addison-Wesley, Reading, MA, 1959), p. 161.

[15] The state called "$L = m$" in Ref. [4] is a mixture of states $L = 0$, $S = 2$ and $L = 2$, $S = 0$ with their respective weight coefficients A_{02} and A_{20} connected by the relation $A_{20} R''_2(0)/A_{02} M^2 R_0(0) = 0.27$. The state called "$L = 2$" is a mixture of states $L = 2$, $S = 0$ and $L = 2$, $S = 2$ with their respective weight coefficients related by $A_{20}/A_{22} = -6.5$. Both mixtures have been adjusted in such a way that they fit the experimental ratios of helicity amplitudes measured in the process $J/\psi \to \gamma f_2(1720)$.

[16] J. Kwiecinski, A. D. Martin, W. J. Stirling, and R. G. Roberts, Phys. Rev. D **42**, 3645 (1990). We chose the parametrization called "B_0" in that paper.

[17] P. Lutz (private communication).

[18] Let us recall that helicities are here defined in the glueball rest frame. The outcome of the computation (i.e., the spectra $d\sigma/dp_T$) is of course independent of the particular frame where the helicities are defined.